Coherent Association of Single Molecules from Single Atoms

A DISSERTATION PRESENTED
BY
YICHAO YU
TO
THE DEPARTMENT OF PHYSICS

IN PARTIAL FULFILLMENT OF THE REQUIREMENTS
FOR THE DEGREE OF
DOCTOR OF PHILOSOPHY
IN THE SUBJECT OF
PHYSICS

HARVARD UNIVERSITY
CAMBRIDGE, MASSACHUSETTS
MARCH 2021

Thesis advisor: Professor Kang-Kuen Ni Yichao Yu

Coherent Association of Single Molecules from Single Atoms

Abstract

Contents

Acknowledgments

,

0

Introduction

1

Apparatus

1.1 Cooling and Optical Pumping Beams

(MOT, OP, fiber back reflection)

(Mention Na Raman beam to be covered in later chapter?)

1.2 Tweezer and Imaging

1.3 Molecular Raman Frequency Generation

(beam path, calibration)

2

Computer Control of the Experiment

2.1 Overall Structure

2.2 Frontend

(Abstraction) (Backward compatibility) (Flexibility) (Text based/version control friendly)

2.3 Backends

(communication protocol) (IR)

2.3.1 FPGA Backend

(clock generation) (pulse merging) (compression)

2.3.2 NiDAQ Backend

(Variable clock)

2.3.3 USRP Backend

(SIMD)

2.4 Automation of Scan

(Scan requirement) (Combination of scans) (Scope/nested structure)

2.5 Summary and Outlook

(new backend/SPCM) (native code generation, auto vectorization) (dynamic logic and dependency tracking/optimization)

3

Raman Sideband Cooling

3.1 Introduction

(In order to achieve full quantum control on molecules, we need to control atoms first.) (An example of such control) (Motional degrees of freedom) (PGC cools to ...) (RSC to further cool.)

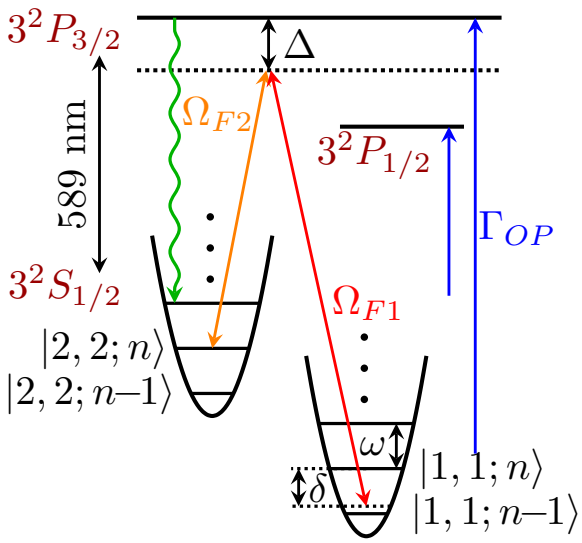

Figure 3.1: Single Na atom Raman sideband cooling scheme. The Raman transitions between $|2,2;n\rangle$ and $|1,1;n+\Delta n\rangle$ have a one-photon detuning $\Delta = 75$ GHz below the $3^2S_{1/2}$ to $3^2P_{3/2}$ transition. Two-photon detuning, δ, is defined relative to the $\Delta n = 0$ carrier transition. For optical pumping, we use two σ^+ polarized transitions, one to pump the atom state out of $|1,1\rangle$ via $3^2P_{3/2}$ and one to pump atoms out of $|2,1\rangle$ via $3^2P_{1/2}$ to minimize heating of the $|2,2\rangle$ state.

3.2 Theory

3.1

3.3 Setup

3.2

3.4 Challenge with Large Lamb-Dicke Parameter

3.3

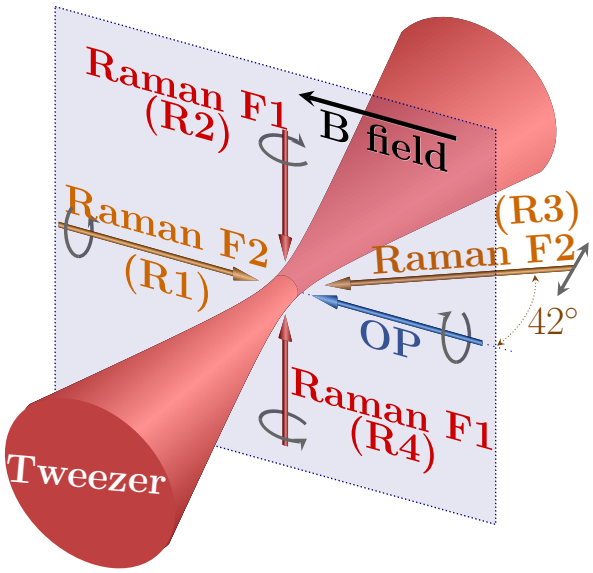

Figure 3.2: Geometry and polarizations of the Raman and optical pumping beams relative to the optical tweezer and bias magnetic field. Raman beams R1 and R4 address the radial x-mode. R1 and R2 address the radial y-mode. R3 and R4 address the axial z-mode, where the beams also couple to radial motion, but this coupling can be neglected when the atoms is cooled to the ground state of motion.

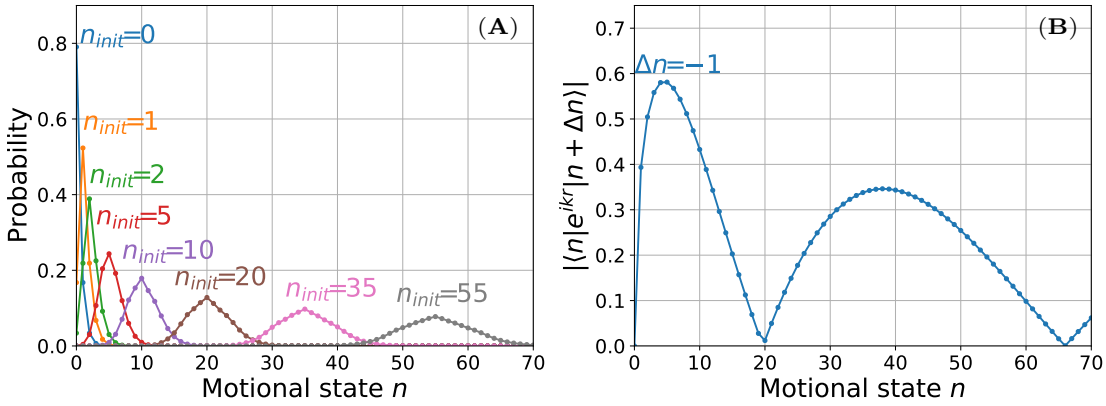

Figure 3.3: Optical pumping motional-state redistribution and Raman coupling for large LD parameters for the axial direction (z). The range plotted covers 95% of the initial thermal distribution. (A) Motional state distribution after one OP cycle for different initial states motion, n_{init}. Due to photon-recoil and the large LD parameter, $\eta_z^{\text{OP}} = 0.55$, there is a high probability of n changing. (B) Matrix elements for Raman transition on the first order cooling sideband deviate from $\sqrt{n}$ scaling with multiple minima.

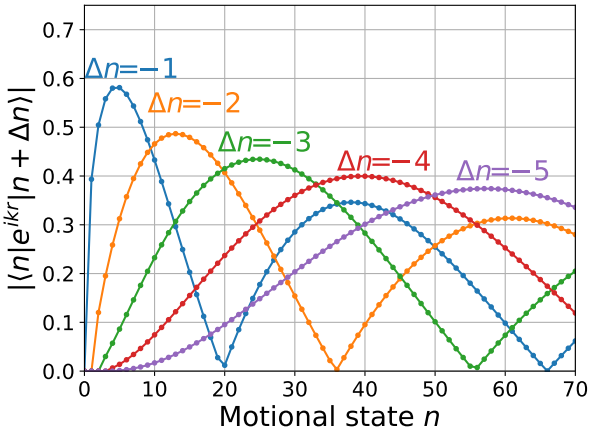

Figure 3.4: Matrix elements for Raman transition including high order sidebands. During cooling, we utilize the fact that high motional states couple most effectively to sidebands with large $|\Delta n|$ in order to overcome the issue with variation and dead zone in the coupling strengths.

3.5 Solution: High Order Sidebands

3.4

3.6 Solution: Simulation Based Optimization

3.5

3.7 Calibration

(Sideband/carrier) (Cold vs hot)

3.8 Cooling Performance

3.6 3.7

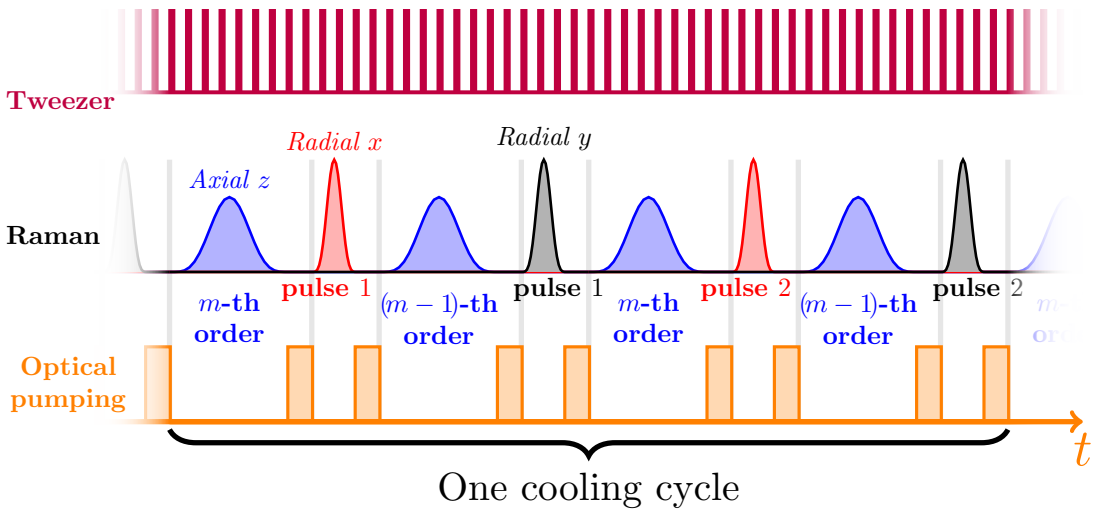

Figure 3.5: Schematic of the cooling pulse sequence. The tweezer is strobed at 3 MHz to reduce light shifts during optical pumping[Hutzler et al.]. Each cooling cycle consists of 8 sideband pulses. The four axial pulses address two sideband orders. The two pulses in each radial direction either address $\Delta n = -2$ and $\Delta n = -1$ or have different durations to drive $\Delta n = -1$, at the end of the cooling sequence when most of the population is below $n = 3$. The Raman cooling and spectroscopy pulses have Blackman envelopes[Kasevich & Chu] to reduce off-resonant coupling, while the measurement Rabi pulses in Fig. 3.7 have square envelopes to simplify analysis.

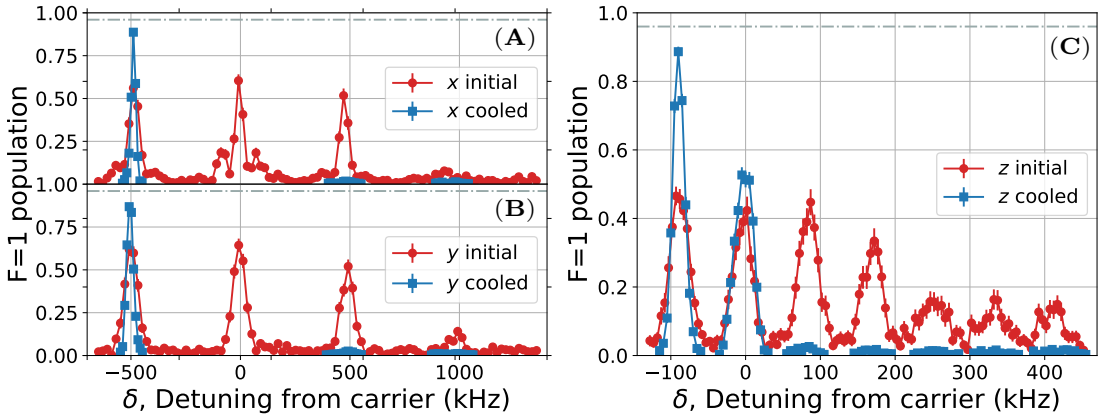

Figure 3.6: Raman sideband spectra for (A) x, (B) y, (C) z axis before (red circle) and after (blue square) applying Raman sideband cooling sequence. The height of the cooling sidebands (positive detuning) are strongly suppressed after cooling which suggests most of the atoms are cooled to the motional ground state in the trap.

Figure 3.7 *(following page)*: Rabi flopping on radial axis x (A) carrier and (B) $\Delta n_x = 1$ sideband, radial axis y (C) carrier and (D) $\Delta n_x = 1$ sideband, axial axis z (E) carrier and (F) $\Delta n_x = 1$ sideband, before (red circle) and after (blue square) Raman sideband cooling.
Solid lines (both red and blue) in all plots are fits to a Rabi-flopping that includes a thermal distribution of motional states [Meekhof et al.] as well as off-resonant scattering from the Raman beams.
The blue lines correspond to a ground state probability of (A-D) 98.1% along radial axis and (E-F) 95% along the axial axis after cooling. The red lines correspond to a thermal distribution of 80 μK before RSC. The horizontal dashed lines in all the plots correspond to the $4\ \%$ probability of imaging loss.
The green dashed line in (F) includes the additional decoherence due to a fluctuation of the hyperfine splitting of magnitude 3 kHz. We see that the decoherence effect is strongest for the post-cooling data on the axial $\Delta n_z = 1$ sideband where the Rabi frequency is the lowest.

Figure 3.7: (continued)

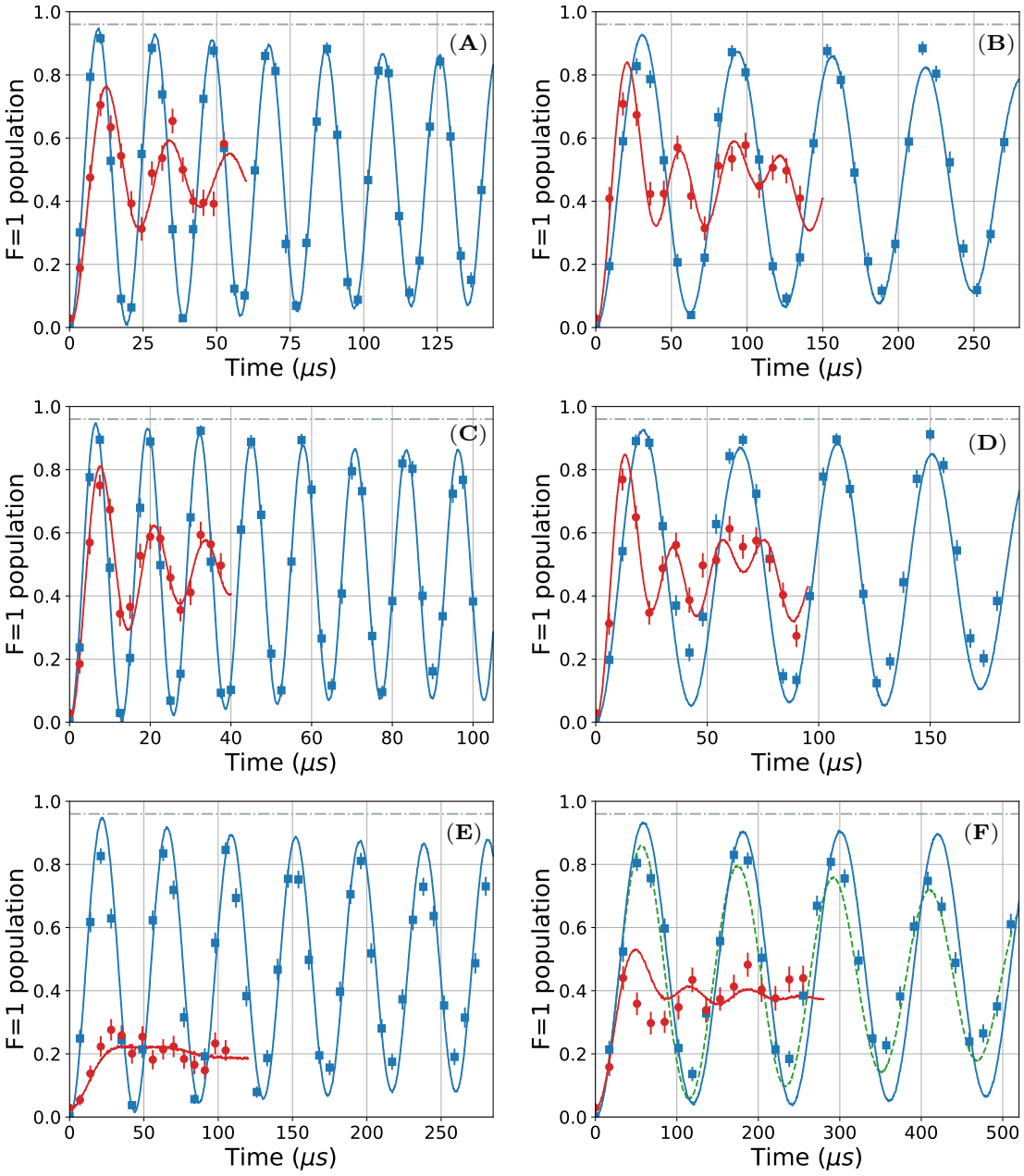

4

Interaction of Single Atoms

4.1 Scattering Length

(Importance/relation with binding energy etc.)

4.2 Energy Levels of Two Interacting Atoms in an Anisotropic Trap

(appendex?)

4.3 Interaction Shift Spectroscopy

(motional sideband, scattering length result)

4.4 Summary and Outlook

(Motional state selection)

5

Photoassociation of Single Atoms

5.1 Energy Levels

5.2 Effect of the Trap

(light shift, broadening)

5.3 Photoassociation Spectroscopy

(v=0, 12, 14, etc)

6

Two-photon Spectroscopy of NaCs

Ground State

7

Coherent Optical Creation of NaCs Molecule

7.1 Introduction

7.2 Raman Transition Beyond Three-Level Model

In an ideal three-level system, the scattering probability during a π pulse Raman transition can be made arbitrarily small by using a large single photon detuning. However, in a real system, there are often other effects that increases the scattering and may also put a lower limit on the scattering probability during the transfer. Other practical limitation in the system like stability of the laser power and frequency also needs to be taken into account. Fig. 7.1 shows a generic model for a real Raman transition demostrating some of these effects. In the experiment, we find the parameter range that gives the best transfer efficiency using numerical simulation (see section 7.4). Nevertheless, in order to develop a general approach that can be applied to other systems, it is also important to understand the various physical mechanism that leads to the optimal parameters. Therefore, in this section, we will discuss some of the most important effects on the transfer efficiency at qualitative and semiquantitative level. Due to experimental constraint, we will assume that the single photon

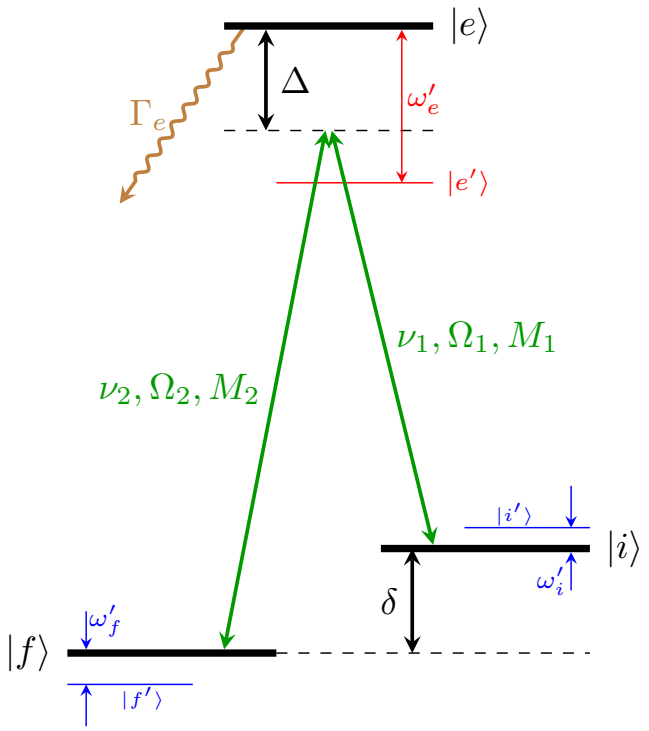

Figure 7.1: Generic model for a real Raman transition. The initial state $|i\rangle$ and the final state $|f\rangle$ has a energy difference δ and are coupled by two Raman beams with frequencies and single photon Rabi frequencies of $\nu_1,\ \Omega_1$ and $\nu_2,\ \Omega_2$ respectively. The corresponding matrix elements (arbitrary unit) are M_1 and M_2. The Raman beams are detuned by Δ from the primary excited state $|e\rangle$, which has a decay rate of Γ_e. We also consider additional states near the initial ($|i'\rangle$), final ($|f'\rangle$) and intermediate excited $|e'\rangle$ states which are separated from the corresponding Raman transition states by ω'_i, ω'_f and ω'_e respectively. Only one additional state of each kinds are included to simplify the discussion without loss of generality.

detuning is much smaller than the frequency of each individual beams, i.e. $\Delta \ll \nu_1,\ \nu_2$.

7.2.1 Additional Initial and Final States

First, we will discuss the effect of $|i'\rangle$ and $|f'\rangle$ states near the initial and final states. These states can be coupled to the excited state $|e\rangle$ by the Raman beams, which can in tern be coupled to the initial and final states by an off-resonance Raman transition. The leakage is suppressed by the detuning

from the Raman resonance, i.e. ω_i' and ω_f'. This puts a limit on the Raman Rabi frequency Ω_R to be smaller than the smallest energy gap, which in turns puts a limit on the minimum Raman transfer time. In our experiment, the minimum energy gap comes from axial motional excitation of the atomic initial states which is between $2\pi \times 10 - 30$ kHz depending on the trap depth used. The typical Raman π time we can realize is $0.5 - 5$ ms so this effect is not a major limiting factor for our transfer efficiency.

7.2.2 Additional Excited states

Next, we will consider the effect of the $|e'\rangle$ state near the excited intermediate state. These states can be coupled to the ground states, both $|i\rangle$ and $|f\rangle$, by the Raman beams and can cause a change in both the Raman Rabi frequency and the scattering rate.

7.2.3 Cross Coupling Between Light Addressing Initial and Final States

7.3 Raman Transfer versus STIRAP

An alternative method often used to create and prepare the internal states of ultracold molecule is stimulated Raman adiabatic passage (STIRAP). Compared to Raman transition, which uses detuning from the excited state to reduce scattering during the transfer, STIRAP relies on a superposition between the initial and final state as a dark state to achieve the same goal. The dark state in STIRAP is created due to a destructive interference of transition from the initial and final state to the excited state.

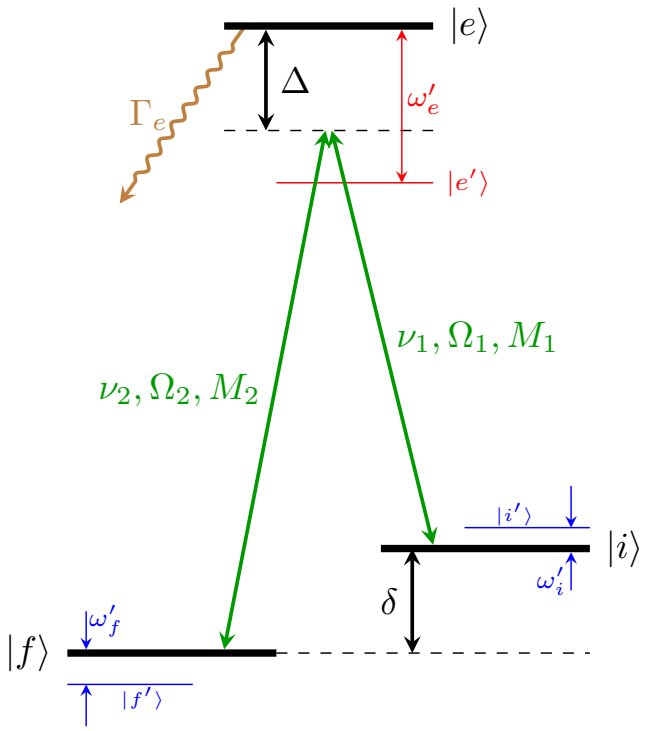

Figure 7.2:

Similar to Raman transfer, STIRAP in an ideal three-level system can achieve full coherent transfer with arbitrarily small scattering probability when given unlimited time and power budget. However, in reality, states and coupling that exist outside the ideal three-level system always have a non-zero probability of scattering loss. In this section, we will apply the approach we took for Raman transition and apply it to STIRAP. We will then compare the loss caused by different practical limitations and discuss which approach should be taken under certain circumstance.

7.3.1 Generic Model for STIRAP

7.2

7.3.2 Additional Initial and Final States

7.3.3 Additional Excited states

7.3.4 Cross Coupling Between Light Addressing Initial and Final States

7.3.5 Conclusion

7.4 States Selection

(Differential Light Shift) (Scattering)

7.4.1 Excited State Selection

7.4.2 Ground States Selection

Final Molecular State

Initial Atomic State

7.5 Raman Transfer Results

7.5.1 Scaling of Raman Transition Parameters

8

Conclusion

A

Computer Control Hardware Specification

NI DAQ

FPGA

DDS

USRP

B

Full Raman Sideband Cooling Sequence

Each Raman pulse in the cooling sequence is followed immediately by an optical pumping pulse. The full parameters for the Raman pulses, including the cooling "axis", the sideband "order (Δn)", the cooling frequency "δ'", the carrier ($\Delta n = 0$) frequency "δ'_0", the pulse "duration", the pulse strength in "Ω_0", and the beam of which a non-uniform "power ramp" is applied, are listed in 6 groups below. The applied cooling frequency, δ', is the two-photon detuning given relative to the

zero-field $F = 1$ and $F = 2$ hyperfine splitting of 1.7716261288(10)GHz[Steck]. Due to the Stark shifts of the Raman beams, the carrier transition, ∂_0', varies with the power of the Raman beams. ∂_0' is given also relative to the zero-field hyperfine splitting. The strength of the pulses given in Ω_0 determines the two-photon Rabi frequency, $\Omega_{n,\Delta n} = \Omega_0 \langle n|e^{i\vec{k}\cdot\vec{r}}|n+\Delta n\rangle$. We adopt the convention that a π-pulse between state n and $n + \Delta n$ requires a duration $\pi/\Omega_{n,\Delta n}$. The difference between ∂' and ∂_0' gives the motional sideband frequency, ∂. Many Raman pulses include a "power ramp" with a Blackman envelope[Kasevich & Chu] to minimize off-resonant excitations. Because each Raman pulse is a product of two spatial- and temporal-overlapped laser beams, the "power ramp" is applied only to the beam that has the smaller light shift (we label the beam by the corresponding F number) while the other beam has a square-pulse shape. For a Raman pulse with a power ramp, the Rabi frequency gives the arithmetic mean over the duration of the pulse.

Group 1

This group is repeated 4 times.

Axis	Δn	δ' (MHz)	δ'_0 (MHz)	Duration (μs)	Ω_0 (kHz)	Power ramp
x	-2	19.625	18.649	44.1	$2\pi \times 23$	F1
y	-2	19.615	18.648	28.6	$2\pi \times 35$	F1
x	-1	19.130	18.649	36.9	$2\pi \times 23$	F1
y	-1	19.615	18.648	24.0	$2\pi \times 35$	F1

Group 2

This group is repeated 5 times.

Axis	Δn	δ' (MHz)	δ'_0 (MHz)	Duration (μs)	Ω_0 (kHz)	Power ramp
z	-5	19.030	18.605	81.5	$2\pi \times 16$	F2
x	-2	19.625	18.649	44.1	$2\pi \times 23$	F1
z	-4	18.940	18.605	76.3	$2\pi \times 16$	F2
y	-2	19.615	18.648	28.6	$2\pi \times 35$	F1
z	-5	19.030	18.605	81.5	$2\pi \times 16$	F2
x	-1	19.130	18.649	36.9	$2\pi \times 23$	F1
z	-4	18.940	18.605	76.3	$2\pi \times 16$	F2
y	-1	19.130	18.648	24.0	$2\pi \times 35$	F1

Group 3

This group is repeated 6 times.

Axis	Δn	δ' (MHz)	δ'_0 (MHz)	Duration (μs)	Ω_0 (kHz)	Power ramp
z	-4	18.940	18.605	76.3	$2\pi \times 16$	F2
x	-2	19.625	18.649	44.1	$2\pi \times 23$	F1
z	-3	18.858	18.605	70.2	$2\pi \times 16$	F2
y	-2	19.615	18.648	28.6	$2\pi \times 35$	F1
z	-4	18.940	18.605	76.3	$2\pi \times 16$	F2
x	-1	19.130	18.649	36.9	$2\pi \times 23$	F1
z	-3	18.858	18.605	70.2	$2\pi \times 16$	F2
y	-1	19.130	18.648	24.0	$2\pi \times 35$	F1

Group 4

This group is repeated 7 times.

Axis	Δn	δ' (MHz)	δ'_0 (MHz)	Duration (μs)	Ω_0 (kHz)	Power ramp
z	-3	18.858	18.605	70.2	$2\pi \times 16$	F2
x	-2	19.625	18.649	44.1	$2\pi \times 23$	F1
z	-2	18.773	18.605	62.7	$2\pi \times 16$	F2
y	-2	19.615	18.648	28.6	$2\pi \times 35$	F1
z	-3	18.858	18.605	70.2	$2\pi \times 16$	F2
x	-1	19.130	18.649	36.9	$2\pi \times 23$	F1
z	-2	18.773	18.605	62.7	$2\pi \times 16$	F2
y	-1	19.130	18.648	24.0	$2\pi \times 35$	F1

Group 5

This group is repeated 10 times.

Axis	Δn	δ' (MHz)	δ'_0 (MHz)	Duration (μs)	Ω_0 (kHz)	Power ramp
z	-2	18.773	18.605	62.7	$2\pi \times 16$	F2
x	-1	19.130	18.649	36.9	$2\pi \times 23$	F1
z	-1	18.685	18.605	52.5	$2\pi \times 16$	F2
y	-1	19.130	18.648	24.0	$2\pi \times 35$	F1
z	-2	18.773	18.605	62.7	$2\pi \times 16$	F2
x	-1	19.130	18.649	70.0	$2\pi \times 23$	F1
z	-1	18.685	18.605	52.5	$2\pi \times 16$	F2
y	-1	19.130	18.648	46.0	$2\pi \times 35$	F1

Group 6

This group is repeated 30 times.

Axis	Δn	δ' (MHz)	δ'_0 (MHz)	Duration (μs)	Ω_0 (kHz)	Power ramp
z	-1	18.683	18.605	78.7	$2\pi \times 11$	F2
z	-1	18.683	18.605	135.0	$2\pi \times 11$	F2
z	-1	18.685	18.605	78.7	$2\pi \times 11$	F2
x	-1	19.130	18.649	36.9	$2\pi \times 23$	F1
y	-1	19.130	18.648	24.0	$2\pi \times 35$	F1
z	-1	18.685	18.605	78.7	$2\pi \times 11$	F2
z	-1	18.685	18.605	135.0	$2\pi \times 11$	F2
z	-1	18.685	18.605	78.7	$2\pi \times 11$	F2
x	-1	19.130	18.649	70.0	$2\pi \times 23$	F1
y	-1	19.130	18.648	46.0	$2\pi \times 35$	F1

References

[Hutzler et al.] Hutzler, N. R., Liu, L. R., Yu, Y., & Ni, K.-K. Eliminating light shifts for single atom trapping. 19(2), 023007.

[Kasevich & Chu] Kasevich, M. & Chu, S. Laser cooling below a photon recoil with three-level atoms. 69(12), 1741–1744.

[Meekhof et al.] Meekhof, D. M., Monroe, C., King, B. E., Itano, W. M., & Wineland, D. J. Generation of Nonclassical Motional States of a Trapped Atom. 76(11), 1796–1799.

[Steck] Steck, D. A. Sodium D Line Data.